Pharmacokinetic/Pharmacodynamic Model-Guided Identification of Hypoxia-Selective 1,2,4-Benzotriazine 1,4-Dioxides with Antitumor Activity: The Role of Extravascular Transport

Michael P. Hay,* Kevin O. Hicks, Frederik B. Pruijn, Karin Pchalek,† Bronwyn G. Siim,‡ William R. Wilson, and William A. Denny

Auckland Cancer Society Research Centre, Faculty of Medical and Health Sciences, The University of Auckland, Auckland 1003, New Zealand

Received June 10, 2007

Pharmacokinetic/pharmacodynamic (PK/PD) modeling has shown the antitumor activity of tirapazamine (TPZ), a bioreductive hypoxia-selective cytotoxin, to be limited by poor penetration through hypoxic tumor tissue. We have prepared a series of 1,2,4-benzotriazine 1,4-dioxide (BTO) analogues of TPZ to improve activity against hypoxic cells by increasing extravascular transport. The 6 substituents modified lipophilicity and rates of hypoxic metabolism. 3-Alkylamino substituents increased aqueous solubility and also influenced lipophilicity and hypoxic metabolism. PK/PD model-guided screening was used to select six BTOs for evaluation against hypoxic cells in HT29 human tumor xenografts. All six BTOs were active in vivo, and two provided greater hypoxic cell killing than TPZ because of improved transport and/or plasma PK. This PK/PD model considers two causes of therapeutic failure (limited tumor penetration and poor plasma pharmacokinetics) often not addressed early in drug development and provides a general strategy for selecting candidates for in vivo evaluation during lead optimization.

Introduction

Hypoxia is recognized as a negative prognostic factor in the treatment of human tumors, compromising the efficacy of radiotherapy in some types of tumors[1–3] and also leading to chemoresistance through multiple mechanisms.[4–6] Hypoxia also imposes an environmental stress on cells, which drives tumor progression, invasion, and metastasis.[7–11] However, the widespread occurrence of hypoxia in tumors presents an opportunity to develop tumor-selective prodrugs that are metabolized to cytotoxic products via bioreductive processes that are inhibited by oxygen.[6,12,13]

Tirapazamine (TPZ,[a] **1**) is a 1,2,4-benzotriazine 3-amine 1,4-dioxide (BTO) bioreductive agent that is selectively toxic to hypoxic cells[14,15] and has recently been evaluated in clinical trials in combination with chemo-radiotherapy.[16–20] TPZ undergoes enzymic one-electron reduction[21] to a radical anion, which in the presence of oxygen is oxidized back to TPZ with the concomitant production of superoxide.[22] At low levels of oxygen, the protonated[23] radical fragments to produce a cytotoxic oxidizing species. This has been postulated to be either the hydroxyl radical[24] or, via elimination of water, a benzotriazinyl radical.[25] Either radical may then react with DNA to produce DNA sugar radicals,[26] leading to DNA breaks[27–33] and to poisoning of topoisomerase II.[34]

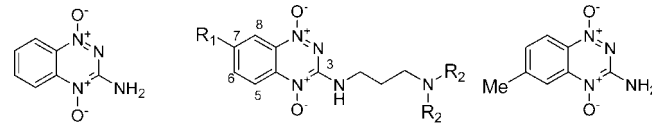

TPZ has a number of limitations that make analogue development a potentially fruitful endeavor. In the clinical setting, TPZ, in combination with radiation and cisplatin, displays significant toxicities.[17–19,35] In addition, TPZ has only moderate solubility, and new analogues with higher solubility (or potency) would be a distinct advantage. Perhaps most importantly, TPZ displays high hypoxic cytotoxicity in vitro (hypoxic cytotoxicity ratio, HCR, ca. 50–100-fold) but a much lower ratio in vivo (2−3-fold).[36] There is considerable evidence from multicellular spheroids and multicellular layer (MCL) culture models that the rapid rate of TPZ metabolism in hypoxic tissue limits extravascular transport (EVT) and that this problem underlies its relatively low hypoxic selectivity in tumors.[37–43] We hypothesize that analogues of TPZ with improved EVT have the potential to provide improved hypoxic selectivity in tumors. In addition, assuming that the normal tissue toxicity of TPZ is less affected by EVT limitations, such analogues can be expected to provide improved therapeutic ratios as anticancer agents. Modeling studies have shown that improving EVT requires optimizing the rate of bioreductive metabolism of TPZ analogues relative to the tissue diffusion coefficient;[44–46] too high a rate will result in excessive metabolic consumption of the prodrug, while too low a rate will compromise the formation of the cytotoxic radical and hence cytotoxic potency.

A previous study described the use of electron-withdrawing substituents at the 7 position of TPZ (**2**; R_1 = F, Cl, CF_3, and NO_2), to increase potency, in combination with high pK_a amine

* To whom correspondence should be addressed: Auckland Cancer Society Research Centre, Faculty of Medical and Health Sciences, The University of Auckland, Private Bag 92019, Auckland 1142, New Zealand. Telephone: 64-9-3737599 ext. 86598. Fax: 64-9-3737502. E-mail: m.hay@auckland.ac.nz.

† Current address: Boehringer Ingelheim Pharma GmbH and Co. KG, 55216 Ingelheim am Rhein, Germany.

‡ Current address: OXiGENE, Inc., Magdalen Centre, Robert Robinson Avenue, The Oxford Science Park, Oxford OX4 4GA, United Kingdom.

[a] Abbreviations: TPZ, tirapazamine; BTO, 1,2,4-benzotriazine 1,4-dioxide; HCR, hypoxic cytotoxicity ratio; MCL, multicellular layer; EVT, extravascular transport; SAR, structure−activity relationship; *E*(1), one-electron reduction potential; PK/PD, pharmacokinetic/pharmacodynamic; D, tissue diffusion coefficient; k_{met}, first-order rate constant for bioreductive metabolism; MTD, maximum-tolerated dose; HCD, hypoxic cytotoxicity differential; $P_{7.4}$, octanol/water coefficient at pH 7.4; CT_{10}, area under the concentration−time curve providing a 10% surviving fraction; M_{10}, amount of BTO metabolized for a 10% surviving fraction; SF, surviving fraction; LCK, log cell kill; $X_{1/2}$, calculated penetration half-distance into hypoxic tissue; AUC_{pred}, area under the plasma concentration−time curve required to give 1 log of cell of hypoxic cells in HT29 tumors.

10.1021/jm070670g CCC: $37.00
Published on Web 11/15/2007

side chains at the 3 position (R_2 = Me and Et) to improve solubility, but these compounds did not show superior in vivo activity to TPZ.[47] We have previously defined in vitro structure–activity relationships (SARs) between one-electron reduction potential, $E(1)$, and in vitro cytotoxicity for BTOs with 5, 6, 7, and 8 substituents that span a wide range of electronic, steric, and hydrophobic properties.[48] This study demonstrated the feasibility of designing compounds with lowered electron affinity resulting from an electron-donating substituent while retaining high hypoxic selectivity (e.g., **3**). However, these studies did not directly address the need to improve EVT requirements in the design of BTOs.

In the present study, we extend the SARs for soluble 3-alkylamino BTOs through the synthesis and evaluation of 43 compounds, with the objective of increasing the in vivo activity by improving EVT. In particular, we use homologation of the 3-alkylamino moiety and variation in amine pK_a to control lipophilicity at neutral pH. We have shown previously, using neutral BTOs, that there is considerable scope to increase the tissue diffusion coefficient of TPZ through analogues with higher lipophilicity.[45] We also use electron-donating substituents in the 6 position to offset the increase in $E(1)$ due to the 3-alkylamino group, thus seeking to optimize rates of bioreductive metabolism in hypoxic tissue.

A general limitation in lead optimization is that empirical SARs for in vivo activity are often only useful retrospectively once a large data set has been obtained. To avoid this problem, we have used a novel tool in the present study, namely, a spatially resolved pharmacokinetic/pharmacodynamic (PK/PD) model that uses EVT parameters measured in vitro (tissue diffusion coefficient, D, determined in MCLs, and the first-order rate constant for bioreductive metabolism in hypoxic cell suspensions, k_{met}) to calculate the drug concentration−time profile at each position in a tumor microvascular network, using the measured plasma PK as input. The model then applies the PK/PD (exposure/cell killing) relationship determined in vitro to calculate the probability of cell kill at each position within the tumor region defined by the microvascular network and to estimate the overall drug-induced kill in the hypoxic subpopulation. We have recently validated this approach by demonstrating its ability to predict the killing of hypoxic cells by TPZ and other BTOs in HT29[43] and SiHa tumors.[46]

In the current study, we apply this spatially resolved PK/PD model as a tool to identify BTOs that are optimized for therapeutic activity against hypoxic cells in tumors. The approach is to measure (or estimate by calculation) the key PK/PD parameters in vitro, for HT29 cells, and use the model to prioritize compounds for initial in vivo evaluation [determination of the maximum-tolerated dose (MTD) and plasma PK]. The measured plasma PK is then used in the model to predict hypoxic cell killing and the differential for hypoxic versus aerobic cells (hypoxic cytotoxicity differential, HCD) in tumors. Analogues predicted by the PK/PD model to show significant hypoxia-selective activity in vivo are then tested against hypoxic cells in HT29 tumor xenografts by evaluating tumor cell killing by the drug following a single dose of ionizing radiation (which selectively kills oxygenated cells). We use this approach to efficiently identify six new BTOs with in vivo activity against hypoxic tumor cells.

Chemistry

Synthesis. Appropriately substituted nitroanilines **4** were condensed with cyanamide under acidic conditions, and the intermediate guanidine ring closed under strongly basic conditions (Scheme 1, General Method A).[48,49] The yields of benzotriazine-3-amine 1-oxides **5** were generally lower for the more lipophilic nitroanilines **4**, primarily because of a separation of the melt in the condensation of **4** with cyanamide. Diazotization of the 1-oxides **5**, using trifluoroacetic acid as the solvent to ensure adequate solubility, gave the intermediate phenols that were converted to 3-chlorides **6** using phosphorus oxychloride with a catalytic amount of DMF (General Method B). The activated chlorides **6** underwent nucleophilic displacement with a variety of amines to give 3-(alkylaminoalkyl)-1-oxides **7** (General Method C). Oxidation of **7** with trifluoroperacetic acid, using trifluoroacetic acid to protect the aliphatic amine from oxidation through protonation, gave the 1,4-dioxides **8–50** (General Method D). This protection strategy was successful for amines with higher pK_a values but was of limited use for morpholides and 3-cyanopyrrolidines with low amine pK_a values. In these instances, side-chain oxidation competed with oxidation at the 4 position and lower yields were generally obtained. Conversion rates to the 1,4-dioxides were generally higher than the isolated yields reported for the reaction, with a difficult chromatographic separation giving a mixed fraction containing starting material and product as well as the reported product fraction. Attempts to drive the reaction to completion resulted in increased decomposition and lower product yields, while the use of different reaction conditions, e.g., adding H_2O_2 to a solution of 1-oxide in either trifluoroacetic or acetic acid also gave lower yields.

Scheme 1[a]

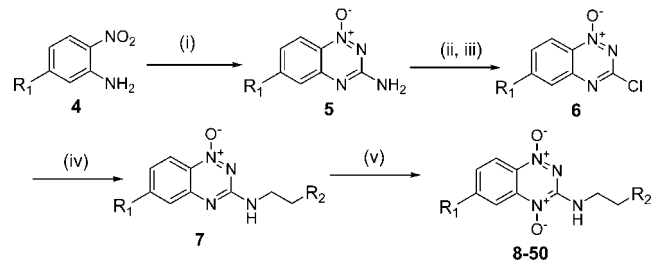

[a] Reagents: (i) NH_2CN, HCl, and then 30% NaOH; (ii) $NaNO_2$, CF_3CO_2H; (iii) DMF, $POCl_3$; (iv) $R_2CH_2CH_2NH_2$, DME; (v) CF_3CO_3H, CF_3CO_2H, DCM.

Physicochemical Measurements. Solubilities of the BTOs **8–50** were determined in culture medium containing 5% fetal calf serum, at 22 °C. Octanol/water partition coefficients were measured at pH 7.4 ($P_{7.4}$) for TPZ, **3**, and a subset of eight BTOs by a low-volume shake flask method, with BTO concentrations in both the octanol and buffer phases analyzed by high-performance liquid chromatography (HPLC) as previously described.[50] These values were used to "train" ACD LogP/LogD prediction software (version 8.0, Advanced Chemistry Development, Inc., Toronto, Canada) using a combination of ACD/LogP System Training and Accuracy Extender. Apparent (macroscopic) pK_a values for the side chain were calculated using ACD pK_a prediction software (version 8.0, Advanced Chemistry Development, Inc., Toronto, Canada).

Biological Methods

In Vitro Assays. Cytotoxic potency was determined by IC_{50} assays, using 4 h drug exposure of HT29 and SiHa cells under aerobic and hypoxic (H_2/Pd anaerobic chamber) conditions in 96-well plates as described previously.[48] The hypoxic cytotoxicity ratio (HCR) was calculated as the intraexperiment ratio of aerobic IC_{50}/hypoxic IC_{50}.

The relationship between cell killing, drug exposure, and drug metabolism (i.e., the in vitro PK/PD model) was determined as

Table 1. Physicochemical, in Vitro, and Modeling Parameters for BTOs **1** and **8–14**[a]

8-14

number	R_1	R_2	pK_a[b]	log $P_{7.4}$ calcd[c]	sol.[d] (mM)	HT29 IC_{50} hypox (μM)	HT29 HCR[e]	SiHa IC_{50} hypox (μM)	SiHa HCR[e]	D calcd[f]	k_{met}[g] (min^{-1})	$X_{1/2}$[h] (μm)	PK/PD model	CT_{10}[i] (μM h)	AUC_{pred}[j] (μM min)	HCD[k]
1	H	na[l]	na[l]	−0.31	8.9	5.1	71	2.5	107	4.17	0.58	45	C × M	24.3	10 300	4.1
8	H	CH_2NMe_2	9.3	−2.01	38	3.4	49	2.3	82	2.40	1.8	18	C × M	7.8	50 300	0.3
9	H	*N*-pyrrole	9.5	−1.34	61	0.6	70	0.2	132	2.77	7.9	10	M	3.6	22 000	0.3
10	H	NMe_2	8.5	−1.02	50	0.7	80	0.2	157	3.38	9.1	10	M	3.2	19 200	0.5
11	H	*N*-morpholine	6.6	−0.48	>49	17.3	34	6.6	44	3.58	0.55	44	C × M	47.5	12 400	5.7
12	H	*N*-piperidine	8.7	−0.46	>49	1.8	24	1.1	55	4.57	6.7	18	C × M	2.8	48 800	0.4
13	H	*N*-2,6-Me_2-piperidine	8.8	−0.21	48	2.2	15	0.9	41	5.53	3.3	25	C × M	5.7	46 700	0.5
14	H	NPr_2	8.7	0.48	>25	1.7	82	2.0	68	10.74	4.9	32	C × M	3.9	16 400	1.4

[a] Error estimates are provided in the Supporting Information. [b] Calculated using ACD pK_a. [c] Calculated using ACD log D. [d] Solubility of HCl salts in culture medium. [e] Hypoxic cytotoxicity ratio = oxic IC_{50}/hypoxic IC_{50}. [f] Diffusion coefficient in HT29 MCLs $\times 10^{-7}$ cm^2 s^{-1}. [g] First-order rate constant for metabolism in anoxic HT29 cell suspensions, scaled to the cell density in MCLs. [h] Penetration half-distance in anoxic HT29 tumor tissue (see the text). [i] Area under the concentration−time curve providing 10% clonogenic survival of hypoxic HT29 cells in vitro. [j] Predicted area under the plasma concentration−time curve required to give 1 log of cell kill of HT29 tumors in addition to that produced by a single 20 Gy dose of γ radiation. [k] In vivo hypoxic cytotoxicity differential = $LCK_{hypoxic}/LCK_{oxic}$ (see the text). [l] Not applicable.

previously described[41,42] by following the clonogenicity of stirred single-cell suspensions of HT29 cells for 3 h, at a drug concentration giving approximately one log kill by 1 h, with the monitoring of drug concentrations in extracellular medium by HPLC. These concentration−time data were fitted to determine the apparent first-order rate constant for metabolic consumption, k_{met}.

The in vitro PK/PD model providing the best fit to the clonogenic assay data was determined as previously described,[42] and the CT_{10} (area under the concentration−time curve providing a 10% surviving fraction) and M_{10} (amount of BTO metabolized for a 10% surviving fraction) were estimated by interpolation. In most cases, the model providing the best fit was one in which the log cell kill was proportional to both the drug concentration and to its cumulative bioreductive metabolism (C × M). This is consistent with the "dual action" mechanism of cell killing by TPZ;[27,30,32] the dependence on cumulative metabolism can be interpreted as reflecting the formation of the reactive free-radical cytotoxin, while the dependence on the BTO concentration can be interpreted as reflecting the oxidation of initial DNA radicals by the BTO.[32,41] Alternatively, cell survival was modeled as either proportional to the amount of BTO metabolized (M) or the square of the amount of BTO metabolized (M^2). The measured parameter values and best fit PK/PD model are given in Tables 1–4, these tables are expanded in the Supporting Information by including the associated error estimates.

Tissue diffusion coefficients, D, of 17 BTOs were measured using HT29 MCLs under 95% O_2 to suppress bioreductive metabolism as previously described.[41] These values, along with previously reported measurements for BTO analogues[42,45] and unpublished data for other BTOs (a total of 73 compounds) were used to develop an algorithm to calculate D for the other analogues.[51] This algorithm extends the reported[45] dependence, for neutral BTOs, of D on log P and molecular weight by replacing log P with the octanol/water distribution coefficient at pH 7.4 (log $P_{7.4}$) and by adding terms for the numbers of hydrogen-bond donors and acceptors. The calculated and measured values and the associated error estimates are tabulated in the Supporting Information. The calculated values for all BTOs are shown in Tables 1–4. There is a good correlation between calculated and measured values of D (using log transformation: slope = 0.885 ± 0.087, $R^2 = 0.874$, $N = 17$, $p < 0.001$), and the standard error of the mean (SEM) and average error (AE) of the estimate (on a linear scale) are 1.27×10^{-7} and 1.19×10^{-7} cm^2 s^{-1}, respectively, which is similar to the mean absolute standard deviation (SD) of the experimental D values of 0.93×10^{-7} cm^2 s^{-1}.

A one-dimensional transport parameter to describe EVT in hypoxic tissue, suitable for ready comparison of BTO analogues, was calculated from the opposing effects of D and k_{met} on tissue transport. The penetration half-distance, $X_{1/2}$, is the distance into a planar one-dimensional hypoxic tissue region at which the BTO concentration falls to half its external value and is calculated as

$$X_{1/2} = \ln(2)\sqrt{\frac{D}{k_{met}}} \quad (1)$$

from the steady-state solution of Fick's second law for diffusion into an infinite plane slab with constant first-order metabolism and constant concentration at the boundary.[52] The calculated values are given in Tables 1–4, and the associated error estimates are tabulated in the Supporting Information.

Table 2. Physicochemical, in Vitro, and Modeling Parameters for 6-Cl-BTOs **15–17** and 6-Me-BTOs **3** and **18–25**[a]

15-25

number	R_1	R_2	pK_a[b]	log $P_{7.4}$ calcd[c]	sol.[d] (mM)	HT29 IC_{50} hypox (μM)	HT29 HCR[e]	SiHa IC_{50} hypox (μM)	SiHa HCR[e]	D calcd[f]	k_{met}[g] (min^{-1})	$X_{1/2}$[h] (μm)	PK/PD model	CT_{10}[i] (μM h)	AUC_{pred}[j] (μM min)	HCD[k]
1	H	na[l]	na[l]	−0.31	8.9	5.1	71	2.5	107	4.17	0.58	45	C × M	24.3	10 300	4.1
15	Cl	NEt_2	9.4	0.08	23	0.3	43	0.2	28	7.31	8.3	18				
16	Cl	*N*-piperidine	8.6	0.16	3.2	0.4	19	0.2	18	7.76	6.7	22				
17	Cl	NPr_2	8.6	1.10	0.6	0.6	9	0.3	21	15.87	9.2	22				
3	Me	na[l]	na[l]	0.08	3.0	12.9	36			5.37	0.20	90	C × M	61.9	6520	9.1
18	Me	NMe_2	8.5	−0.77	>51	1.9	159	1.1	200	3.78	1.5	28	C × M	6.3	4280	3.3
19	Me	NEt_2	9.5	−0.08	>49	1.0	51	0.3	35	6.45	1.9	32	C × M	8.3	11 300	1.6
20	Me	*N*-morpholine	6.6	−0.05	>46	21.8	55	8.3	86	5.03	0.31	65	C × M	134.0	34 100	6.1
21	Me	*N*-piperidine	8.7	0.00	45	4.0	58	2.2	75	6.85	1.4	39	C × M	9.4	8150	2.4
22	Me	CH_2−*N*-morpholine	7.3	0.22	43	15.5	25	5.4	46	5.56	0.38	66	C × M	67.8	13 900	6.7
23	Me	CH_2−*N*-pyrrol-3-CN	7.7	−0.13	49	14.1	54	9.2	54	4.13	0.50	62	C × M	62.2	21 000	4.6
24	Me	*N*-2,6-Me_2-piperidine	8.8	0.25	48	2.8	126	0.8	159	8.37	1.2	47	C × M	15.4	17 100	2.4
25	Me	NPr_2	8.7	0.94	38	2.7	108	0.6	149	14.89	1.4	54	M[2]	38.6	11 700	7.3

[a–l] See Table 1.

In Vivo Assays. BTO analogues were formulated as their hydrochloride salts in 0.9% saline, 5% dimethylsulfoxide (DMSO)/saline, or lactate buffer (pH 4.0) as specified in Table 5. All in vivo studies used single i.p. doses of BTOs in CD-1 homozygous nude mice. The MTD was determined using 1.33-fold dose increments and defined as the highest dose not causing mortality, body weight loss (>15%), or other severe morbidity in any of the 6 mice. Plasma PK of the total drug was measured at 75 or 100% of MTD by HPLC, and the noncompartmental PK parameters AUC, C_{max} (maximum drug concentration), and $t_{1/2}$ (drug half-life) were determined. Plasma protein binding was found to be negligible for a representative subset of compounds (**1**, **11**, **14**, **18**, and **39**; see Table 5 in the Supporting Information), for which this was measured by equilibrium dialysis, as previously described.[43] The measured plasma concentrations were therefore assumed to reflect free drug concentrations.

Activity against hypoxic cells in HT29 tumor xenografts was determined by an excision assay following treatment of mice with the test drug 5 min after a dose of γ radiation (20 Gy) large enough to sterilize the oxic cells in the tumor. Tumors were excised 18 h later, and single-cell suspensions were prepared and plated to determine the number of surviving clonogens/g of tumor. Surviving fractions (SF) were calculated as the ratio of treated/control clonogens/g of tumor, and drug-induced logs of hypoxic cell kill (LCK) was calculated as

$$\text{hypoxic LCK} = \log(\text{SF, radiation}) - \log(\text{SF, radiation plus drug}) \quad (2)$$

Spatially Resolved PK/PD Model. The spatially resolved PK/PD model for BTOs has been described in detail recently.[42,53] Briefly, transport is modeled in the extravascular compartment of a representative tumor microvascular network by solving the Fickian diffusion-reaction equations using a Green's function method. The transport parameters used in the model are the tissue diffusion coefficient D (estimated in MCLs) and k_{met} (scaled to MCL cell density) determined in vitro as above. The input to the extravascular compartment is provided by the measured plasma-free drug PK (AUC, C_{max}, $t_{1/2}$). The resulting description of micropharmacokinetics (concentration−time profile) at each point in the 3D tissue microregion is used, in conjunction with the homogeneous PK/PD model established in vitro for each compound, to predict LCK at each position. The predicted overall cell kill through the whole tumor region is calculated for the drug plus 20 Gy radiation and for radiation only (using the reported radiosensitivity parameters for aerobic and hypoxic HT29 cells).[42] The difference between these gives the model-predicted logs of hypoxic cell kill (LCK_{pred}). In addition, the hypoxic cytotoxicity differential (HCD) is calculated by the model as a measure of hypoxic selectivity in the tumor

$$\text{HCD} = \frac{\text{LCK in the hypoxic region (<4 } \mu\text{M O}_2)}{\text{LCK in the well-oxygenated region (>30 } \mu\text{M O}_2)} \quad (3)$$

where LCK is predicted for the drug alone (without radiation).

PK/PD Model-Guided Testing Algorithm. A schematic of the testing algorithm, guided by the spatially resolved PK/PD model, is shown in Figure 1. BTOs were tested in the IC_{50} assay, and the HCR was determined. In general, only BTOs with a HCR > 20 against either HT29 or SiHa cells were advanced to further study. Diffusion coefficients, D, in MCLs were measured or calculated, and in vitro metabolism/cytotoxicity experiments determined k_{met}, CT_{10}, and M_{10} values. The in vitro PK/PD

Table 3. Physicochemical, in Vitro, and Modeling Parameters for 6-Alkyl-BTOs **26–38**[a]

26-38

number	R_1	R_2	pK_a[b]	log $P_{7.4}$ calcd[c]	sol.[d] (mM)	IC_{50} hypox (μM)	HT29 HCR[e]	IC_{50} hypox (μM)	SiHa HCR[e]	D calcd[f]	k_{met}[g] (min^{-1})	$X_{1/2}$[h] (μm)	PK/PD model	CT_{10}[i] (μM h)	AUC_{pred}[j] (μM min)	HCD[k]
1	H	na[l]	na[l]	−0.31	8.9	5.1	71	2.5	107	4.17	0.58	45	C × M	24.3	10 300	4.1
26	Et	NMe_2	8.5	−0.23	>49	1.3	116	0.5	186	5.73	2.8	24	C × M	6.2	11 400	0.8
27	Et	*N*-piperidine	8.7	0.53	39	1.5	65	1.0	50	11.01	4.0	28	M^2	11.9	6990	3.4
28	Et	CH_2−*N*-morpholine	7.4	0.72	55	10.4	>36	5.6	66	9.07	0.38	84	C × M	56.5	9560	8.2
29	iPr	NMe_2	8.5	0.12	42	1.9	120	1.1	104	7.84	1.99	34	C × M	11.6	16 500	1.7
30	iPr	NEt_2	9.5	0.80	45	2.0	122	0.8	113	13.56	2.69	38	C × M	18.6	14 200	4.9
31	iPr	*N*-morpholine	6.7	0.83	30	45.1	14	15.5	33	11.03	0.30	104	C × M	217.8	59 900	9.8
32	iPr	*N*-piperidine	8.7	0.88	18	2.7	41	1.1	65	14.08	1.85	47	C × M	15.2	12 000	2.9
33	iPr	NPr_2	8.7	1.82	39	4.4	35	0.9	65	20.38	1.61	61	C × M	41.6	19 900	4.4
34	tBu	NMe_2	8.5	0.46	38	3.7	99	1.1	78	12.48	1.4	42	C × M	11.4	6120	3.3
35	tBu	NEt_2	9.5	1.15	>48	4.3	37	0.9	90	13.57	1.8	47	C × M	33.1	21 600	3.3
36	tBu	*N*-piperidine	8.7	1.23	28	4.0	31	0.6	121	16.80	1.73	50	C × M	30.3	17 000	3.8
37	tBu	*N*-morpholine	6.7	1.30	1.8	61.2	13	10.9	55	1.41						
38	tBu	NPr_2	8.7	2.16	32	8.3	18	3.8	35	22.27	1.54	57	M^2	66.6	16 900	4.7

[a–l] See Table 1.

relationship was used to predict the area under the plasma concentration−time curve (AUC_{pred}) that would be required to give 1 log of cell kill in addition to that produced by a single 20 Gy dose of γ radiation and also to predict the HCD. In general, in vivo testing was only undertaken for those compounds that were predicted to have a HCD > 1 and an AUC_{pred} below an arbitrary threshold of <20 000 μM.min. The latter value is ca. 7-fold higher than that for TPZ (Table 5) and, therefore, unlikely to be achievable by an analogue at well-tolerated doses. Determination of MTD and plasma PK parameters (AUC, C_{max}, and $t_{1/2}$) for BTOs allowed use of the spatially resolved PK/PD model to predict the achievable LCK (LCK_{pred}). In general, only those compounds with LCK_{pred} > 0.5 were tested for antitumor activity in vivo, although two examples predicted to be inactive (**14** and **50**) and three examples of borderline predicted activity (**11**, **45**, and **49**), were also tested, to further evaluate the predictive value of the model.

Results and Discussion

In Vitro Studies. The initial set of soluble BTOs **8–14** based on literature examples, e.g., **2**,[47] provided increased hypoxic potency and rates of hypoxic metabolism (k_{met}), relative to TPZ (Table 1). This increase in cytotoxic potency is caused, in part, by an increase in electron affinity because of the 3-alkylamino substituent, with the one-electron reduction potential, $E(1)$, of **10** (−396 mV[26]), 60 mV higher than TPZ (−456 mV).[48] Only the nearly neutral morpholide **11** showed lower cytotoxic potency and metabolism than TPZ. The BTOs **8–14** were hypoxia-selective. The diffusion coefficient (D) in MCLs increased with increasing lipophilicity, but only the three most lipophilic compounds (**12**, **13**, and **14**) displayed better D values than TPZ, reflecting the liability, in terms of diffusion, of a polar amine as a solubilizing side chain.

The calculated penetration half-distance into hypoxic tissue ($X_{1/2}$, μm) is a simple descriptor of EVT. None of the alkylamino BTOs **8–14** has better EVT properties than TPZ. The increases in lipophilicity in **12**, **13**, and **14** were not sufficient to overcome increases in metabolism. Only the morpholide **11**, with a similar D value and k_{met} to TPZ, had a similar $X_{1/2}$ value, but this came at the expense of hypoxic potency and selectivity.

We hypothesized that the diffusion liability of the solubilizing side chains in **8–14** might be offset by combining lipophilic substituents at the 6 position with lipophilic amines of moderate pK_a. Two approaches were taken to explore this possibility. In the first, 6-chloro substituents were combined with three lipophilic amines, BTOs **15–17** (Table 2). Although the electron-withdrawing 6-chloro substituent has been shown to raise the reduction potential[48] and, hence, a higher k_{met} would be expected, the possibility that this could be offset by the lipophilicity of the chloro group, leading to a high D, was examined.

Aqueous solubility was lowered for the 6-chloro-BTOs, and although increased hypoxic potency and metabolism were seen, the increases in diffusion were not sufficient to offset the effect of increased hypoxic metabolism on EVT, resulting in low $X_{1/2}$ values for **15–17**.

The second approach used electron-donating 6-methyl substituents to lower rates of metabolism and increase lipophilicity simultaneously. The prototype for this approach, **3**, displays a 2-fold increase in EVT. This is a consequence of the increase in lipophilicity and, thus, diffusion, coupled with a decreased electron affinity [$E(1)$ = –493 mV[48]] and hypoxic metabolism (Table 2). We prepared analogues of **3** with lipophilic amine side chains **18–25**, in which the increases in lipophilicity

Table 4. Physicochemical, in Vitro, and Modeling Parameters for 6-Alkoxy-BTOs **39–50**[a]

39-50

number	R_1	R_2	pK_a[b]	log $P_{7.4}$ calcd[c]	sol.[d] (mM)	HT29 IC_{50} hypox (μM)	HT29 HCR[e]	SiHa IC_{50} hypox (μM)	SiHa HCR[e]	D calcd[f]	k_{met}[g] (min^{-1})	$X_{1/2}$[h] μm	PK/PD model	CT_{10}[i] (μM h(	AUC_{pred}[j] (μM min)	HCD[k]
1	H	na[l]	na[l]	−0.31	8.9	5.1	71	2.5	107	4.17	0.58	45	C × M	24.3	10 300	4.1
39	MeO	NMe_2	8.5	−0.76	46	7.7	89	2.9	232	2.87	0.54	35	C × M	26.1	13 800	2.7
40	MeO	*N*-morpholine	6.6	−0.11	48	103.0	>39	40.9	70	2.66	0.05	139				
41	MeO	*N*-piperidine	8.6	−0.53	45	10.8	24	3.0	65	3.16	0.33	61	C × M	38.9	4900	7.8
42	MeO	CH_2−*N*-morpholine	7.4	−0.35	>44	22.0	>8	10.2	447	2.77	0.29	60	C × M	149.7	35 800	5.7
43	MeO	CH_2−*N*-pyrrole-3-CN	7.7	−0.29	47	40.6	41	31.9	36	2.82	0.11	105	C × M	211.4	27 700	9.9
44	MeO	2,6-Me_2-piperidine	8.8	−0.27	29	3.9	34	1.0	121	3.61	0.53	53	C × M	26.1	7320	4.4
45	EtO	NMe_2	8.5	−0.23	>50	2.6	121	0.8	245	3.77	0.40	52	M[2]	50.1	12 300	7.9
46	EtO	*N*-piperidine	8.6	0.00	>49	2.2	116	1.7	169	4.58	0.48	64	C × M	36.3	10 200	5.1
47	EtO	CH_2−*N*-morpholine	7.4	0.18	>51	18.0	52	7.6	140	3.79	0.11	120	C × M	260.6	32 600	9.7
48	$MeOC_2O$	NMe_2	8.5	−1.09	>51	5.0	162	1.6	401	2.20	0.61	32	C × M	22.3	15 500	2.3
49	iPrO	NMe_2	8.5	0.12	>55	6.2	35	3.2	31	4.88	0.58	49	C × M	45.1	14 800	4.5
50	CPMO[m]	NMe_2	8.5	−0.39	43	3.8	117	2.1	101	4.88	0.74	44	C × M	51.8	15 600	3.7

[a–l] See Table 1. [m] Cyclopropylmethoxy.

generally translated into increased diffusion (Table 2). Although, the 6-methyl substituent lowered the electron affinity of the BTO nucleus [the $E(1)$ of **18** (−440 mV[26]) was 44 mV lower than **10**], the contribution of the side chain pK_a to hypoxic cytotoxicity (linear regression of log IC_{50} versus pK_a gave $R^2 = 0.90$ and $p < 0.001$ for HT29 and $R^2 = 0.81$ and $p < 0.01$ for SiHa) and metabolism (logk_{met} versus pK_a gave $R^2 = 0.90$ and $p > 0.001$) tended to dominate, keeping k_{met} elevated relative to TPZ. Only BTOs with weakly basic amine side chains (e.g., **20**, **22**, and **23**) had k_{met} values lower than TPZ, which translated into greater EVT than for TPZ. The most lipophilic compounds **24** and **25** had sufficiently large diffusion coefficients to offset their high k_{met} values and, consequently, also had modestly improved EVT relative to TPZ.

We expanded the range of electron-donating 6 substituents to include ethyl, *iso*-propyl, and *tert*-butyl groups, BTOs **26–38** (Table 3). The increased lipophilicity of **26–38** resulted in generally lower solubility than their corresponding 6-methyl homologues, but with the exception of **37**, this was still greater than TPZ. All compounds were hypoxia-selective. The increased lipophilicity of **26–38** is reflected in increased diffusion coefficients with up to a 5-fold increase in D values compared to TPZ. The 6-alkyl BTOs displayed similar hypoxic cytotoxicity and metabolism compared to their 6-methyl homologues, although the 6-ethyl analogues **26** and **27** were notably higher. Again, a fine balance between the rate of hypoxic metabolism and the diffusion coefficient exists for simple substituent variations. Modest gains in EVT occur within an amine homologous series (e.g., compare **18**, **26**, **29**, and **34**) with increased lipophilicity compensating for relatively high hypoxic metabolism. Large increases in EVT are seen for the morpholides **28** and **31**, where significant increases in D are not accompanied by increased k_{met} values, although this advantage is offset by a loss in cytotoxic potency (high IC_{50} and CT_{10} values).

The above observations indicate that the electronic effect of 6-alkyl substituents may not be sufficient to adjust the rate of metabolism into the optimal range, providing only modest gains in EVT. This prompted us to explore 6-alkoxy BTOs **39–50**, with a stronger electronic influence, to further dampen hypoxic metabolism (Table 4). The electron-donating 6-methoxy substituent lowers the reduction potential of **39** to −500 mV,[26] and cytotoxic potencies for the alkoxy BTOs were relatively low, especially with weakly basic side chains as demonstrated by **40**, **42**, **43**, and **47** (linear regression of log IC_{50} versus pK_a gave $R^2 = 0.80$ and $p < 0.0001$ for HT29 and $R^2 = 0.78$ and $p < 0.001$ for SiHa). The more polar alkoxy substituents generally lowered lipophilicity and gave lowered diffusion coefficients. However, this was balanced by low rates of hypoxic metabolism and led, with the exception of **39** and **48**, to compounds with equal (**44** and **50**) or improved EVT properties compared to TPZ. Compound **40** clearly demonstrates how a relatively low diffusion coefficient can be balanced by slowing the rate of hypoxic metabolism sufficiently to improve EVT. Unfortunately, the rate of hypoxic metabolism of **40** is so low that the potency of the compound is severely impaired.

Modeling. The in vitro PK/PD relationship, combined with the estimates of EVT properties, was used in the spatially resolved PK/PD model to calculate AUC_{pred} (the area under the plasma concentration−time curve required to give 1 log of cell of hypoxic cells in HT29 tumors) and HCD (the predicted hypoxic cytotoxicity differential in these tumors) for **1** and **8–14**, using a C × M cell survival model in most cases (Table 1). TPZ gave a modest value for AUC_{pred} and was calculated to

Table 5. In Vivo Parameters for Selected BTOs

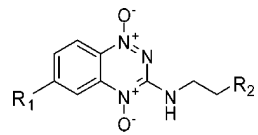

									plasma pharmacokinetics			log cell kill, HT29 tumors: drug only[a]				log cell kill, HT29 tumors: RT plus drug[b]			
number	R_1	R_2	$X_{1/2}$[c] (μm)	AUC_{pred}[d] (μM min)	HCD[e]	form[f]	MTD[g] (μmol kg^{-1})	dose[h] (μmol kg^{-1})	C_{max} (μM)	$t_{1/2}$ (min)	AUC (μM min)	mean	SEM	p	pred[i]	mean	SEM	p
1	H	na[j]	45	10 300	4.1	A	178	133	61.7	27.9	2950	0.15	0.08	ns	0.31	0.59	0.15	0.01
3[k]	Me	na[j]	90	6520	9.1	B	1000	1000	198.5	34.1	11 300	0.39	0.11	ns	1.92	2.16	0.15	0.01
11	H	*N*-morpholine	44	12 400	5.7	C	562	562	159.9	16.5	6280	0.29	0.05	ns	0.35	0.60	0.36	ns[l]
14	H	NPr_2	32	16 400	1.4	B	316	316	17.0	11.8	430	0.01	0.09	ns	0.05	0.25	0.07	ns[l]
18	Me	NMe_2	28	4280	3.3	B	562	562	103.8	22.5	4140	0.07	0.06	ns	0.98	1.00	0.14	0.01
20	Me	*N*-morpholine	65	34 100	6.1	C	1000	750	131.9	15.4	5210				0.10			
21	Me	*N*-piperidine	39	8150	2.4	C	237	237	14.9	16.6	830				0.01			
22	Me	CH_2−*N*-morpholine	65	13 900	6.7	C	1000	750	237.8	34.0	11 700	0.13	0.06	ns	0.99	1.28	0.11	<0.01
24	Me	*N*-2,6-Me_2-piperidine	47	17 100	2.4	C	421	421	19.6	19.1	1100				0.02			
25	Me	NPr_2	54	10 200	4.5	C	421	316	3.8	17.3	156				0.00			
26	Et	NMe_2	24	11 400	0.8	C	421	316	21.6	12.7	789				0.05			
28	Et	CH_2−*N*-morpholine	83	9550	8.2	A	1000	750	139.3	24.9	5690	0.13	0.08	ns	0.59	0.82	0.32	0.049
34	tBu	NMe_2	42	8050	2.6	C	421	421	16.1	12.5	584				0.04			
39	MeO	NMe_2	35	13 800	2.7	C	1000	1000	157.0	51.5	14 400	0.15	0.04	0.04	1.60	1.84	0.16	<0.01
41	MeO	*N*-piperidine	53	4900	7.8	A	421	316	26.7	24.6	1210				0.08			
45	EtO	NMe_2	52	12 300	7.9	A	1000	750	85.7	31.6	4940	0.09	0.13	ns	0.29	0.83	0.31	0.041
46	EtO	*N*-piperidine	52	10 200	5.1	C	316	237	9.8	40.1	643				0.00			
48	$MeOC_2O$	NMe_2	32	15 500	2.3	A	1330	1000	164.0	44.9	15 400	−0.08	0.01	ns	1.01	0.53	0.15	0.019
49	iPrO	NMe_2	49	14 800	4.5	A	1330	1000	123.2	26.1	6130	−0.17	0.09	ns	0.40	−0.06	0.14	ns[l]
50	CPMO[m]	NMe_2	44	15 600	3.7	A	750	562	48.6	33.9	3080	−0.14	0.14	ns	0.07	0.30	0.18	ns[l]

[a] In comparison to unirradiated controls treated with the vehicle only. [b] In comparison to radiation alone. [c] Penetration of the half-distance in anoxic HT29 tumor tissue (see the text). [d] Predicted area under the plasma concentration−time curve required to give 1 log of cell kill in addition to that produced by a single 20 Gy dose of γ radiation. [e] In vivo hypoxic cytotoxicity differential = $LCK_{hypoxic}/LCK_{oxic}$. [f] Formulation: A, 0.9% saline; B, 5% DMSO/saline; C, 0.1 M sodium lactate buffer at pH 4. [g] Maximum tolerated single i.p. dose. [h] Dose given for pharmacokinetic and activity assays. [i] Predicted log cell kill, in addition to radiation, from the PK/PD model; other columns are measured values. [j] Not applicable. [k] Data from ref 43. [l] Not significant, $p > 0.05$. [m] Cyclopropylmethoxy.

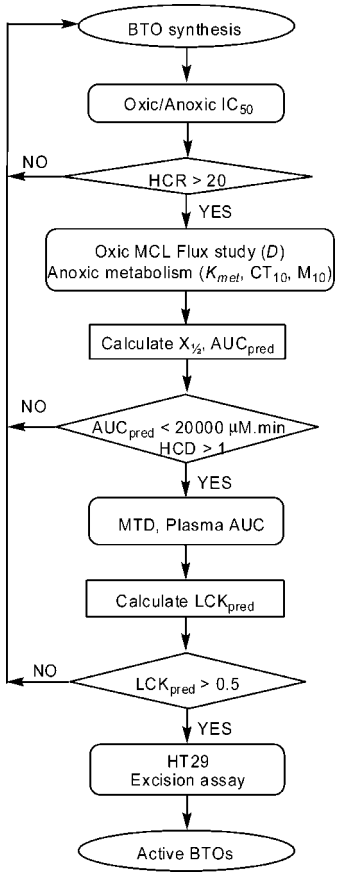

Figure 1. Flowchart of PK/PD model-guided drug design of BTOs.

have a HCD consistent with its observed in vivo activity.[42,43] Modeling predictions gave AUC_{pred} values that were realistic (<20 000 μM min) for only the NMe_2 **10**, morpholide **11**, and dipropylamine **14**. Only BTO **11** was predicted to be hypoxia-selective in vivo, with the low selectivity a consequence of the poor EVT for most of this set of analogues. Model predictions for BTOs **18**–**25** gave modest AUC_{pred} requirements for all compounds, with the exception of **20** and **23**, which both have very weak amine side chains and low cytotoxic potencies (Table 2). All of the BTOs were predicted to display hypoxic selectivity in vivo, but only the weaker bases **20**, **22**, and **23** gave predicted HCD values greater than TPZ. Modeling predictions for **26**–**38** gave almost a 10-fold range in the required AUC_{pred} (Table 3). The AUC_{pred} values for 6-ethyl BTOs **27** and **28** as well as 6-*tert*-butyl BTO **34** were potentially achievable in vivo. High hypoxic selectiviy was calculated for the weak bases **28** (HCD 8.2) and **31** (HCD 9.8); however, the latter was not sufficiently potent, and a very high AUC_{pred} was calculated. Calculation of AUC_{pred} for **39**–**50** revealed that most 6-alkoxy BTOs had values below the threshold of 20 000 μM min, with the exception of the very weak bases **42**, **43**, and **47** (Table 4). These along with piperidine **41** and the 6-ethoxy BTOs **45** and **46** were predicted to be more selective in vivo than TPZ (HCD > 4.1).

In Vivo Studies. Generally, BTOs passing the thresholds for AUC_{pred} (<20 000 μM min) and HCD (>1) were advanced to in vivo testing. A number of lipophilic compounds (e.g., **19**, **23**, **27**, **29**, **30**, **32**, **33**, **35**, **36**, **38**, and **44**) meeting the criteria were not progressed to in vivo testing because of close structural similarity to analogues with demonstrated low MTDs. MTDs were determined in CD-1 nude mice, and plasma AUC, C_{max}, and $t_{1/2}$ values of potential candidates were measured (Table 5). Without exception, BTOs meeting the selection criteria were better tolerated than TPZ. Although there was no obvious trend across the whole data set, within a homologous series, e.g., the 6-methyl-BTOs (**18**, **20**, **21**, **22**, **24**, and **25**), the more lipophilic compounds **21**, **24**, and **25** were more toxic in vivo than the morpholides **20** and **22** (Table 5). Similarly, for a series of homologous amines, e.g., in the C_2NMe_2 series (**18**, **26**, and **34**), the more lipophilic analogues displayed increased toxicity in vivo. The relationship between lipophilicity and animal toxicity was less clear in the alkoxy series (**39**, **45**, **48**, **49**, and **50**), where subtle structural changes made significant changes in toxicity; e.g., cyclopropylmethoxide **50** was more toxic than isopropoxide **49**. A comparison of pairs of homologues shows a decrease in vivo toxicity with a decreasing electron affinity. Thus, the 6-H BTOs **11** and **14** were more toxic than the corresponding 6-Me BTOs **20** and **25**; similarly, 6-Me BTOs **18** and **21** were more toxic than the corresponding 6-MeO BTOs **39** and **41**.

Initially, the plasma PK parameters were determined at the MTD; however, because of the risk of toxicity when treating tumor-bearing animals at these doses and to avoid potential nontargeted effects, such as acute blood flow changes,[54] measurements were subsequently conducted at 75% of MTD. Taking this difference into account, we estimate that 9 of 17 compounds gave higher AUC values than TPZ at equivalent toxicity. However, when considered as a ratio of the injected dose, the AUC values across the whole compound set ranged from 2 to 70% of that for TPZ. This PK liability (at least for intraperitoneal dosing) seemed to be the least for BTOs with weakly basic morpholide side chains (**11**, **20**, **22**, and **28** with AUC/dose ratios of 50, 31, 70, and 34% of TPZ, respectively), although stronger bases also appeared to be acceptable if the overall lipophilicity was not too high (e.g., **18**, **39**, and **48** with AUC/dose ratios of 33, 65, and 69% of TPZ, respectively).

The plasma PK was used as an input to the spatially resolved PK/PD model to generate a prediction of LCK_{pred} (the predicted log cell kill of hypoxic tumor cells). BTOs with $LCK_{pred} > 0.5$ were tested for in vivo activity against HT29 tumors. Two examples that were predicted to be inactive (**14** and **50**) and three borderline examples (**11**, **45**, and **49**) were also tested in vivo to further evaluate the predictive power of the model.

A single dose of BTO was given 5 min after a high dose (20 Gy) of radiation, which was designed to sterilize the oxic compartment of the tumor. Drug efficacy was assessed by ex vivo determination of clonogenic survival 18 h after treatment with the drug alone (overall tumor cell kill) and the drug following radiation (hypoxic cell kill). The additional cell kill seen over radiation alone represents the killing of hypoxic tumor cells (logs of hypoxic cell kill, LCK) by the BTO (Figure 2 and Table 5). None of the BTOs showed any single-agent activity in keeping with the proposed mechanism of action. TPZ, given at 133 μmol kg^{-1} (75% of MTD) or 178 μmol kg^{-1} (100% of MTD), gave hypoxic LCKs of 0.59 log and 0.95 log, respectively. We have previously shown[43] that **3**, when administered at 1000 μmol kg^{-1} (100% of MTD), had a higher activity (LCK, 2.16 $\pm$ 0.15) than TPZ against hypoxic cells in HT29 tumors, consistent with the PK/PD model predictions. However, because of low aqueous solubility, this compound was administered as a suspension. In contrast, the new BTOs were all sufficiently soluble to administer in solution. As expected, BTOs **14** and **50** with low LCK_{pred} values (0.0 and 0.1, respectively) did not display any significant in vivo activity. BTOs with borderline LCK_{pred} values, e.g., **11**, **45**, and **49**, showed mixed activity, with **11** and **49** inactive and **45** displaying modest activity. Six BTOs (**18**, **22**, **28**, **39**, **45**, and **48**) with LCK_{pred} >

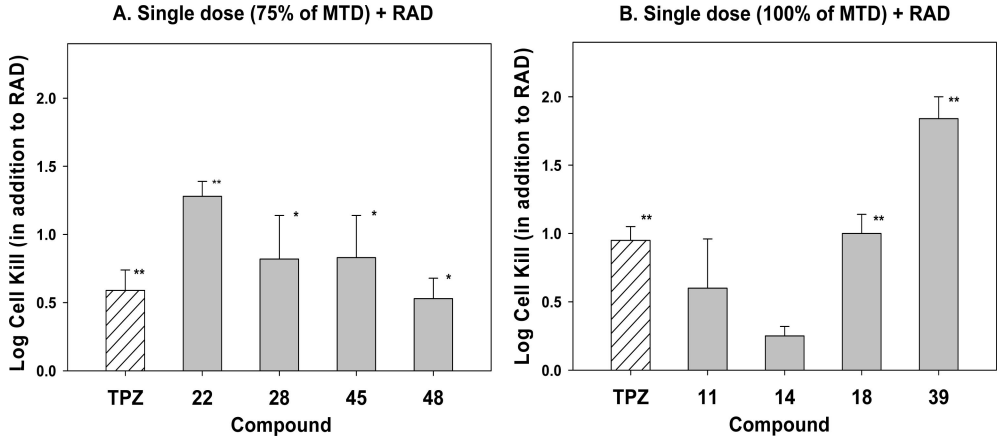

Figure 2. In vivo activity of BTOs against hypoxic cells in human tumor xenografts following single i.p. dosing of mice. Hypoxic cell killing was determined as [log(clonogens/g of tumor radiation only)] − [log(clonogens/g of tumor radiation plus drug)]. p values versus RAD: (*) $p < 0.05$, (**) $p < 0.01$. (A) Drug given at 75% of MTD 5 min after irradiation of HT29 tumors. (B) Drug given at 100% of MTD 5 min after irradiation of HT29 tumors.

0.5 displayed significant in vivo activity with radiation, with **18** and **39** being given at the MTD and the other four BTOs given at 75% of their MTD.

The 6-Me-BTO **22** and the 6-MeO-BTO **39** displayed the greatest activity in the HT29 tumor model. Although **22** had lower in vitro hypoxic potency and selectivity than TPZ, improved EVT resulting from increased diffusion and lowered metabolism combined with a favorable PK profile to deliver increased in vivo activity. The increased diffusion resulted from the addition of the lipophilic methyl group, loss of one hydrogen-bond donor, and the use of a low basicity morpholine group for solubility. These structural changes also resulted in lowered hypoxic metabolism. BTO **39** has similar in vitro hypoxic potency and selectivity to TPZ. However, its polar methoxy group, in combination with a more basic amine group, lowered diffusion without sufficiently lowering metabolism, resulting in reduced EVT. However, this was offset by a favorable plasma PK profile, leading to the observed in vivo activity.

There was good agreement between the LCK predicted by the PK/PD model and the LCK observed in HT29 tumors (correlation coefficient, $R^2 = 0.78$, and $p < 0.001$), confirming the model validation reported previously for a different set of TPZ analogues.[43] Interestingly, the in vivo activity of three of the six active BTOs (**22**, **28**, and **39**) would not have been predicted by the usual in vitro criteria of improving hypoxic potency ($IC_{50} < 5.1$ μM) and selectivity (HCR > 71) relative to TPZ. Conversely, if these in vitro criteria were used to select candidates for in vivo testing, then 14 of 43 candidates (**9**, **10**, **14**, **18**, **24**–**26**, **29**, **30**, **34**, **45**, **46**, **48**, and **50**) would have qualified, but on the basis of our PK/PD modeling, we would predict that all, except **18**, **45**, and **48**, would have been found to be inactive. This use of the PK/PD model therefore represents a significant improvement in screening for bioreductive antitumor agents.

Conclusions

We prepared 3-alkylamino BTO analogues of TPZ to increase aqueous solubility and EVT. While basic amine side chains conferred increased solubility, high pK_a amines limited EVT by increasing hypoxic metabolism and reducing diffusion. These effects on EVT could be countered by using lipophilic, electron-donating 6 substituents, with the best balance being achieved in the combination of 6-alkyl groups with near neutral morpholide side chains, e.g., **20**, **22**, **28**, and **31**. More deactivating 6-alkoxy substituents were required to balance elevated hypoxic metabolism when the more basic amine side chains, such as NMe_2 and *N*-piperidine were used, leading to analogues with improved EVT, such as **41**, **42**, **45**, and **46**. The 1D transport parameter $X_{1/2}$ allowed for a ready comparison of substituent effects on EVT.

Predictive modeling of plasma AUC values required for in vivo activity provided a rational basis for selection of BTOs for in vivo testing. Using this approach, plasma PK parameters were then measured at or near the MTD and used to predict hypoxic log cell kill (LCK_{pred}) and thus prioritize BTOs for the measurement of activity against hypoxic tumor cells in mice. BTO analogues with higher lipophilicity and in vitro cytotoxic potency were generally also more toxic in vivo, allowing only moderate plasma concentrations and LCK_{pred} values to be achieved, thus compromising many BTOs with high EVT. PK/PD modeling gave reliable predictions of hypoxic LCK in vivo and identified six soluble BTOs (**18**, **22**, **28**, **39**, **45**, and **48**) with activity against hypoxic cells in HT29 tumors. BTOs **22** and **39** displayed similar activity in the HT29 xenograft model to that seen previously by administering suspensions of the insoluble compound **3**. Relative to TPZ, BTO **22** displayed increased EVT and improved plasma PK at equivalent host toxicity resulting in increased in vivo activity, despite having reduced in vitro cytotoxic potency and selectivity. In the case of BTO **39**, lower EVT was offset by improved plasma PK, again resulting in superior in vivo activity relative to TPZ.

Thus, PK/PD-guided screening of BTOs has proven useful in efficiently identifying in vivo active compounds. It explicitly considers two important causes of therapeutic failure in this class, which are not usually included in early drug development, that of limited tumor tissue penetration and poor plasma pharmacokinetics. Importantly, it provides a rational strategy for selecting compounds for evaluation in resource-intensive therapeutic studies in advance of establishing the SAR for in vivo activity. The spatially resolved PK/PD-guided approach is likely to have broader application in lead optimization, especially in cases where there are nonlinear terms in the SAR, such as the present study, where there is a need to optimize rather than maximize rates of prodrug metabolism in the target

tissue to balance the competing requirements of prodrug distribution and activation.

Experimental Section

Chemistry. General experimental details are described in the Supporting Information. TPZ[55] and BTO **3**[48] were synthesized as previously described.

Example of Synthetic Methods. See the Supporting Information for full experimental details of compounds **8**–**50**.

Preparation of 3-Amino-1,2,4-benzotriazine 1-Oxides 5. General Method A. A mixture of nitroaniline **4** (20 mmol) and cyanamide (80 mmol) were mixed together at 100 °C, cooled to 50 °C, cHCl (10 mL), added dropwise (CAUTION: exotherm), and the mixture was heated at 100 °C for 4 h. The mixture was cooled to 50 °C; a 7.5 M NaOH solution was added until the mixture was strongly basic; and the mixture was stirred at 100 °C for 3 h. The mixture was cooled, diluted with water (100 mL), filtered, washed with water (3 × 30 mL), washed with ether (2 × 5 mL), and dried. If necessary, the residue was purified by chromatography, eluting with a gradient (0–10%) of MeOH/dichloromethane (DCM), to give amine **5**.

6-Ethoxy-1,2,4-benzotriazin-3-amine 1-Oxide (106). Method A. Reaction of nitroaniline **105** (1.63 g, 9.0 mmol) gave amine **106** (1.26 g, 68%) as a yellow powder. mp (MeOH) 268–271 °C. ^{1}H NMR [$(CD_3)_2SO$] δ: 8.02 (d, J = 9.4 Hz, 1 H, H-8), 7.19 (br s, 2 H, NH_2), 6.92 (dd, J = 9.4, 2.6 Hz, 1 H, H-7), 6.83 (d, J = 2.6 Hz, 1 H, H-5), 4.17 (q, J = 7.0 Hz, 2 H, CH_2O), 1.37 (t, J = 7.0 Hz, 3 H, CH_3). ^{13}C NMR [$(CD_3)_2SO$] δ: 163.9, 160.7, 151.2, 124.8, 121.4, 117.1, 104.2, 64.2, 14.1. Anal. Calcd for $C_9H_{10}N_4O_2$: C, 52.4; H, 4.9; N, 27.2. Found: C, 52.4; H, 4.8; N, 27.0.

Preparation of 3-Chloro-1,2,4-benzotriazine 1-Oxides 6. General Method B. Sodium nitrite (10 mmol) was added in small portions to a stirred solution of amine **5** (5 mmol) in trifluoroacetic acid (20 mL) at 0 °C, and the solution was stirred at 20 °C for 3 h. The solution was poured into ice/water, stirred 30 min, filtered, washed with water (3 × 10 mL), and dried. The solid was suspended in $POCl_3$ (20 mL) and DMF (0.2 mL) and stirred at 100 °C for 1 h. The solution was cooled, poured into ice/water, stirred for 30 min, filtered, washed with water (3 × 30 mL), and dried. The solid was suspended in DCM (150 mL) and dried, and the solvent evaporated. The residue was purified by chromatography, eluting with 5% EtOAc/DCM, to give chloride **6**.

3-Chloro-6-ethoxy-1,2,4-benzotriazine 1-Oxide (107). Method B. Reaction of amine **106** (1.05 g, 5.1 mmol) gave chloride **107** (813 mg, 71%) as a pale yellow solid. mp (EtOAc/pet. ether) 150–153 °C. ^{1}H NMR δ: 8.28 (d, J = 9.5 Hz, 1 H, H-8), 7.30 (dd, J = 9.5, 2.6 Hz, 1 H, H-7), 7.17 (d, J = 2.6 Hz, 1 H, H-5), 4.22 (q, J = 7.0 Hz, 2 H, CH_2O), 1.53 (t, J = 7.0 Hz, 3 H, CH_3). ^{13}C NMR δ: 165.6, 157.7, 150.2, 128.8, 124.1, 121.8, 106.2, 65.2, 14.3. Anal. Calcd for $C_9H_8ClN_3O_2$: C, 47.9; H, 3.6; N, 18.6; Cl, 15.7. Found: C, 48.2; H, 3.5; N, 18.7; Cl, 15.8.

Preparation of 1-Oxides 7. General Method C. Amine (3.0 mmol) was added to a stirred solution of chloride **6** (1.0 mmol) in 1,2-dimethoxyethane (DME, 50 mL), and the solution was stirred at reflux temperature for 8 h. The solution was cooled to 20 °C; the solvent evaporated; and the residue partitioned between aqueous NH_4OH solution (100 mL) and EtOAc (100 mL). The organic fraction was dried, and the solvent evaporated. The residue was purified by chromatography, eluting with a gradient (0–10%) of MeOH/DCM, to give 1-oxide **7**.

***N*^{1}-(6-Ethoxy-1-oxido-1,2,4-benzotriazin-3-yl)-*N*^{2},*N*^{2}-dimethyl-1,2-ethanediamine (108). Method C.** Reaction of *N*,*N*-dimethylethanediamine (0.48 mL, 4.4 mmol) and chloride **107** (327 mg, 1.5 mmol) in DME (50 mL) gave 1-oxide **108** (390 mg, 97%) as a yellow solid. mp (MeOH/EtOAc) 152–153 °C. ^{1}H NMR δ: 8.14 (d, J = 9.4 Hz, 1 H, H-8), 6.85 (dd, J = 9.4, 2.6 Hz, 1 H, H-7), 6.82 (d, J = 2.6 Hz, 1 H, H-5), 5.90 (br s, 1 H, NH), 4.14 (q, J = 7.0 Hz, 2 H, CH_2O), 3.54 (br dd, J = 5.8, 5.6 Hz, 2 H, CH_2N), 2.56 (br t, J = 5.9 Hz, 2 H, CH_2N), 2.28 [s, 6 H, $N(CH_3)_2$], 1.48 (t, J = 7.0 Hz, 3 H, CH_3). ^{13}C NMR δ: 164.8, 159.6, 151.5, 125.9, 122.0, 118.0, 104.4, 64.4, 57.5, 45.1 (2), 38.7, 14.5. Anal. Calcd for $C_{13}H_{19}N_5O_2 \cdot {}^1/_4H_2O$: C, 55.4; H, 7.0; N, 24.9. Found: C, 55.6; H, 6.7; N, 25.2.

Preparation of 1,4-Dioxides 8–50. General Method D. Hydrogen peroxide (70%, 10 mmol) was added dropwise to a stirred solution of trifluoroacetic anhydride (10 mmol) in DCM (20 mL) at 0 °C. The mixture was stirred at 0 °C for 5 min, warmed to 20 °C, stirred for 10 min, and cooled to 5 °C. The mixture was added to a stirred solution of 1-oxide **7** (1.0 mmol) and trifluoroacetic acid (TFA, 5.0 mmol) in DCM (15 mL) at 0 °C, and the mixture was stirred at 20 °C for 16 h. The solution was carefully diluted with water (20 mL), and the mixture was made basic with aqueous NH_4OH solution, stirred for 15 min, and then extracted with $CHCl_3$ (5 × 50 mL). The organic fraction was dried, and the solvent evaporated. The residue was purified by chromatography, eluting with a gradient (0–15%) of MeOH/DCM, to give 1,4-dioxide **8**–**50**.

***N*^{1}-(6-Ethoxy-1,4-dioxido-1,2,4-benzotriazin-3-yl)-*N*^{2},*N*^{2}-dimethyl-1,2-ethanediamine (45). Method D.** Oxidation of 1-oxide **108** (385 mg, 1.4 mmol) with CF_3CO_3H (ca. 13.9 mmol) gave 1,4-dioxide **45** (125 mg, 31%) as a red solid. mp (MeOH/EtOAc) 150–152 °C. ^{1}H NMR δ: 8.23 (d, J = 9.6 Hz, 1 H, H-8), 7.48 (d, J = 2.6 Hz, 1 H, H-5), 7.46 (br s, 1 H, NH), 7.03 (dd, J = 9.6, 2.6 Hz, 1 H, H-7), 4.25 (q, J = 7.0 Hz, 2 H, CH_2O), 3.64 (br dd, J = 6.0, 5.9 Hz, 2 H, CH_2N), 2.61 (t, J = 6.0 Hz, 2 H, CH_2N), 2.30 [s, 6 H, $(CH_3)_2$], 1.49 (t, J = 7.0 Hz, 3 H, CH_3). ^{13}C NMR δ: 165.5, 150.2, 140.3, 125.6, 123.5, 120.6, 95.4, 65.4, 57.5, 45.2 (2), 35.9, 14.3. MS−FAB$^+$ (m/z): 294 (MH^+, 100%), 278 (30), 276 (20). HRMS−FAB$^+$ (MH^+) (m/z): calcd for $C_{13}H_{19}N_5O_3$, 294.1566; found, 294.1568. Anal. Calcd for $C_{13}H_{19}N_5O_3$: C, 53.2; H, 6.5; N, 23.9. Found: C, 53.1; H, 6.3; N, 23.6.

Partition Coefficients. The octanol–water partition coefficient ($P_{7.4}$) was measured using the shake flask method, using GPR-grade octanol (BDH Laboratory Supplies).[50] Briefly, hydrophilic drugs were dissolved directly in octanol-saturated phosphate-buffered saline (PBS) (137 mM NaCl, 2.68 mM KCl, 1.47 mM KH_2PO_4, and 8.10 mM Na_2HPO_4 at pH 7.4), and lipophilic drugs were dissolved directly in PBS-saturated octanol, to 25–100 μM. Equal volumes of PBS and octanol were mixed on a Bellco roller drum (Bellco Glass, Inc., Vineland, NJ) at 20 rpm for 3 h at ambient temperature. The two solvent layers were separated after a brief spin and analyzed by HPLC directly (aqueous layer) or after the addition of 4 volumes of methanol (organic layer).

MCL Cultures. MCLs were grown from human HT29 colon carcinoma cells as described elsewhere.[41] In brief, 1 × 10^6 cells were seeded on collagen-coated Teflon microporous support membranes (Biopore; average thickness of 30 μm) in Millicell-CM cell culture inserts (Millipore Corporation, Bedford, MA) and grown for 3 days submerged in stirred culture medium (αMEM; GIBCO BRL, Grand Island, NY) supplemented with 10% heat-inactivated fetal calf serum (GIBCO BRL, Auckland, New Zealand), penicillin (100 units/mL), streptomycin (100 μg/mL), and 2 mM L-glutamine.

Determination of Diffusion Coefficient, *D*, in MCLs. Flux through MCLs was measured in a diffusion chamber as described,[56] using MCLs equilibrated for 60 min with 95% O_2/5% CO_2 at 37 °C in the same medium as above. BTOs were added to the "donor" compartment to 50 μM, along with the reference compounds [^{14}C]urea (Amersham Pharmacia Biotech; 40 MBq/mmol, 7.5 kBq/mL), D-[2-^{3}H]mannitol (ICN Pharmaceuticals, Inc., Irvine, CA; 40 MBq/mmol, 20 kBq/mL), and 9(10*H*)-acridone (Sigma-Aldrich, Castle Hill, New South Wales, Australia; 10 μM). Samples were taken from both the donor and receiver compartment for up to 5 h. An aliquot was assayed for radioactivity by dual-label liquid scintillation counting in a Packard Tri-Carb 1500 liquid scintillation analyzer (Packard Instrument Company, Meriden, CT) using Emulsifier-Safe water-accepting scintillant (Packard), and the balance was frozen for subsequent HPLC analysis. The concentration−time profiles of [^{14}C]urea in the donor and receiver compartments were numerically fitted to Fick's second law to estimate the average thickness of each MCL (ca. 175 μm), using the measured value of D for [^{14}C]urea in HT29 MCLs.[41] The

effective diffusion coefficient of each compound was also determined in the collagen-coated Teflon porous support membrane (D_s) without a MCL present. This latter parameter also takes into account the effect of the unstirred boundary layers on each side of the membrane or MCL. D was then determined by fitting the concentration−time profile in both the donor and receiver simultaneously to a Fickian diffusion model, with the support membrane and MCL in series, as described previously,[56] with the addition of reaction terms in the MCL when necessary.

HPLC. Samples (200 μL) were deproteinized by the addition of 4 μL of 70% (v/v) perchloric acid and chilling on ice followed by centrifugation (12000*g* for 5 min at 4 °C) and subsequent neutralization of the supernatant with 50% (v/v) ammonia (31.5 μL/mL supernatant). Concentrations of the BTOs were determined by reversed-phase HPLC (Alltima C_8 5 μm column, 150 × 2.1 mm; Alltech Associated, Inc., Deerfield, IL) using an Agilent HP1100 equipped with a diode-array detector. Mobile phases were gradients of 80% acetonitrile/20% H_2O (v/v) in 450 mM ammonium formate at pH 4.5 and 0.3 mL/min. Quantitation was based on calibration curves in the mobile phase (0.1–100 μM), corrected for recovery from medium with serum determined by assaying known concentrations (0.1–100 μM) for each compound under the same conditions.

IC_{50} Assays. IC_{50} assays were determined for BTOs under aerobic and hypoxic conditions as previously described.[48] For each experiment, compounds were simultaneously tested under both oxic and hypoxic conditions (the latter using a H_2/Pd catalyst anaerobic chamber) against the HT29 and SiHa cell lines using a 4 h drug exposure and including TPZ as an internal control. In all cases, 8-methyl-5-nitroquinoline was used as a second internal control to confirm that strict hypoxia was present during the experiment.[57] Plates were grown for 5 days after washing out drugs and stained with sulforhodamine B,[58] and IC_{50} values were determined. Final data were pooled from a series of seven independent experiments and were calculated using interexperimental means.

Metabolism Experiments. The potency of BTOs toward hypoxic HT29 cells was also assessed using the loss of colony-forming potential (clonogenicity) as the end point to enable a direct comparison with measurements of activity in tumors, and metabolic consumption of the compounds was assessed in the same experiments as described previously for TPZ.[41] Suspensions of HT29 cells (10 mL at 1 or 2 × 10^6 cells mL^{-1}) were incubated in αMEM without serum in magnetically stirred 20 mL bottles under flowing 5% CO_2/95% N_2 for 90 min. Drugs were then introduced using deoxygenated DMSO stock solutions to give initial concentrations in the medium (C_0) providing approximately 10% cell survival after 1 h. DMSO-only controls were included in each experiment. Samples (0.5 mL) were removed at intervals (typically, at 5 min, 30 min, 1 h, 2 h, and 3 h) and centrifuged to remove cells, and the supernatant stored at −80 °C for subsequent HPLC analysis. The cell pellet was resuspended in fresh αMEM with 5% fetal bovine serum (FBS), and serial dilutions were made into 5 mL of this medium in 60 mm diameter cell-culture dishes. These were incubated at 37 °C for 14 days and stained with methylene blue, and colonies (>50 cells) were counted to determine the plating efficiency (PE). The surviving fraction was calculated for each time as PE (treated)/PE (controls). Cell viability was checked with a hemocytometer at the end of the drug exposure by their ability to exclude 0.4% trypan blue and was >85% in all experiments. Oxygen in solution was checked using an OxyLite 2000 O_2 luminescent fiber-optic probe (Oxford Optronix Ltd., U.K.) by methods previously described,[41] and oxygen concentrations were <0.1 μM O_2 in all cases. A reference vial with TPZ (30 μM) was also included in all experiments for quality control.

Determination of MTD. MTD was determined as the highest dose causing no drug-related deaths in a group of 6 mice with mean body weight loss at day 5 of <10%. Dose escalation was based on an 8-step logarithmic dose scale ($10^{1/8}$-fold = 1.33-fold increments). Mice were observed daily, and any clinical signs were recorded. Mice were weighed daily for the first 5 days and culled if their weight fell below 15% their initial weight, and experiments were terminated at 28 days.

Plasma Pharmacokinetics. Concentrations of total drug (free and bound) in the plasma of CD-1 nude mice were determined, after i.p. dosing at 75 or 100% of the MTD. Small (20–40 μL) blood samples were obtained serially by puncturing the lateral tail vein of anaesthetized restrained animals (typically, at 15 min, 30 min, 1 h, and 2 h) and collecting from a droplet of blood with heparinized hematocrit tubes. Blood was centrifuged immediately to separate plasma, and plasma was frozen for subsequent HPLC analysis. The area under the drug concentration−time curve (AUC_∞), the maximum concentration (C_{max}), and the terminal half-life ($t_{1/2}$) were calculated using noncompartmental analysis (WinNonLin version 4.0, Pharsight Corp.).

Plasma Protein Binding. Drug plasma protein binding was determined by equilibrium dialysis in 50% mouse plasma (diluted 1:1 with PBS) with three replicated determinations typically at 2 concentrations within the range defined by the PK study, by equilibrating for 3 h in a Dianorm multiequilibrium dialyzer (Diachema AG, Rüschlikon-Zürich, Switzerland), with 20 two-cell dialysis chambers (1 mL each), with Cuprophan dialysis membranes at 37 °C. Samples from both sides of the dialysis chamber were stored at −80 °C and analyzed by HPLC. To check for drug loss during the equilibrium dialysis (e.g., nonspecific binding to the apparatus and/or membranes) and extraction efficiency, samples were also prepared in triplicate in 50% mouse plasma and PBS and processed without dialysis. The measured free fraction in 50% mouse plasma (θ_{50}) was scaled to that for 100% mouse plasma (θ) assuming that the total drug concentration is much less than the concentration of binding sites in the blood (and thus the binding site concentration is constant)

$$\theta = \theta_{50}/(2 - \theta_{50})$$

Excision Assay. HT29 tumors were grown by inoculating 10^7 cells, prepared by dissociating HT29 multicellular spheroids, subcutaneously on the back of CD-1 nude mice. When tumors reached a size of approximately 300 mg (average of two largest diameters of 7–10 mm), drugs were administered as single i.p. doses, at the same dose levels as used for the PK studies. The following groups were included in each experiment. A, vehicle control; B, test drug; C, γ radiation (20 Gy); D, TPZ (133 or 178 μmol/kg) 5 min after radiation; and E, test drug 5 min after radiation. Mice in groups C−E received whole-body irradiation from a cobalt-60 source, without anesthesia or restraint. Each group included 3 (A and B) or 4–6 (C−E) mice. Tumors were excised 18 h after treatment, dissociated enzymatically, and plated to determine the number of surviving (clonogenic) cells/g of tumor tissue as described.[59] Drug-induced hypoxic cell kill was determined by the difference between groups C and E, while a comparison of groups A and B evaluates oxic cell killing. Statistical significance of drug effects was evaluated by one-way analysis of variation (ANOVA), using Dunnett's test to determine p values for comparisons between treated and control groups. Surviving fractions (SF) were calculated as the ratio of treated/control clonogens/g of tumor, and drug-induced hypoxic cell kill were calculated as

$$\text{hypoxic LCK} = \log(\text{SF, radiation}) - \log(\text{SF, radiation plus drug})$$

Acknowledgment. The authors thank Jane Botting, Dr. Maruta Boyd, Rachel Chapman, Anna Chappell, Alfred Degenkolbe, Alison Hogg, Sisira Kumara, Sarath Liyanage, and Joanna Sturman for technical assistance. The authors also thank Degussa Peroxide Ltd., Morrinsville, New Zealand, for the generous gift of 70% hydrogen peroxide. This work was supported by the U.S. National Cancer Institute under Grant IP01-82566 (M.P.H., K.O.H., F.B.P., K.P., W.R.W., and W.A.D.), the Health Research Council of New Zealand (W.R.W.), the Cancer Society of New Zealand (B.G.S.), and the Auckland Division of the Cancer Society of New Zealand (W.A.D.).

Supporting Information Available: Experimental details and characterization data for synthetic intermediates and BTOs **8–50**. Tables of physicochemical and in vitro data with estimates of errors. This material is available free of charge via the Internet at http://pubs.acs.org.

References

(1) Nordsmark, M.; Overgaard, M.; Overgaard, J. Pretreatment oxygenation predicts radiation response in advanced squamous cell carcinoma of the head and neck. *Radiother. Oncol.* **1996**, *41*, 31–39.

(2) Fyles, A. W.; Milosevic, M.; Wong, R.; Kavanagh, M. C.; Pintilie, M.; Sun, A.; Chapman, W.; Levin, W.; Manchul, L.; Keane, T. J.; Hill, R. P. Oxygenation predicts radiation response and survival in patients with cervix cancer. *Radiother. Oncol.* **1998**, *48*, 149–156.

(3) Koukourakis, M. I.; Bentzen, S. M.; Giatromanolaki, A.; Wilson, G. D.; Daley, F. M.; Saunders, M. I.; Dische, S.; Sivridis, E.; Harris, A. L. Endogenous markers of two separate hypoxia response pathways (hypoxia inducible factor 2 α and carbonic anhydrase 9) are associated with radiotherapy failure in head and neck cancer patients recruited in the CHART randomized trial. *J. Clin. Oncol.* **2006**, *24*, 727–735.

(4) Durand, R. E. The influence of microenvironmental factors during cancer therapy. *In Vivo* **1994**, *8*, 691–735.

(5) Tannock, I. F. Conventional cancer therapy: Promise broken or promise delayed. *Lancet* **1998**, *351* (Suppl 2), 9–16.

(6) Brown, J. M.; Wilson, W. R. Exploiting tumor hypoxia in cancer treatment. *Nat. Rev. Cancer* **2004**, *4*, 437–447.

(7) Harris, A. L. Hypoxia—A key regulatory factor in tumour growth. *Nat. Rev. Cancer* **2002**, *2*, 38–47.

(8) Semenza, G. L. HIF-1 and tumor progression: Pathophysiology and therapeutics. *Trends Mol. Med.* **2002**, *8*, S62–S67.

(9) Pennachietti, S.; Michieli, P.; Galluzzo, M.; Mazzone, M.; Giordano, S.; Comoglio, P. M. Hypoxia promotes invasive growth by transcriptional activation of the met protooncogene. *Cancer Cell* **2003**, *3*, 347–361.

(10) Cairns, R. A.; Hill, R. P. Acute hypoxia enhances spontaneous lymph node metastasis in an orthotopic murine model of human cervical carcinoma. *Cancer Res.* **2004**, *64*, 2054–2061.

(11) Subarsky, P.; Hill, R. P. The hypoxic tumour microenvironment and metastatic progression. *Clin. Exp. Metastasis* **2003**, *20*, 237–250.

(12) Brown, J. M.; Giaccia, A. J. The unique physiology of solid tumors: Opportunities (and problems) for cancer therapy. *Cancer Res.* **1998**, *58*, 1408–1416.

(13) Denny, W. A.; Wilson, W. R.; Hay, M. P. Recent developments in the design of bioreductive drugs. *Br. J. Cancer* **1996**, *74*, S32–S38.

(14) Brown, J. M. SR 4233 (tirapazamine): A new anticancer drug exploiting hypoxia in solid tumours. *Br. J. Cancer* **1993**, *67*, 1163–1170.

(15) Denny, W. A.; Wilson, W. R. Tirapazamine: A bioreductive anticancer drug that exploits tumour hypoxia. *Expert Opin. Invest. Drugs* **2000**, *9*, 2889–2901.

(16) Peters, L. J.; Rischin, D.; Hicks, R. J.; Hughes, P. G.; Sizeland, A. M. Extraordinary tumor control in phase I trial of concurrent tirapazamine cisplatin and radiotherapy for far advanced head and neck cancer. *Int. J. Radiat. Oncol., Biol., Phys.* **1999**, *45*, 148–149.

(17) Rishin, D.; Peters, L.; Hicks, R.; Hughes, P.; Fisher, R.; Hart, R.; Sexton, M.; D'Costa, I.; von Roemeling, R. Phase I trial of concurrent tirapazamine, cisplatin, and radiotherapy in patients with advanced head and neck cancer. *J. Clin. Oncol.* **2001**, *19*, 535–542.

(18) Rischin, D.; Peters, L.; Fisher, R.; Macann, A.; Denham, J.; Poulsen, M.; Jackson, M.; Kenny, L.; Penniment, M.; Corry, J.; Lamb, D.; McClure, B. Tirapazamine, cisplatin, and radiation versus fluorouracil, cisplatin, and radiation in patients with locally advanced head and neck cancer: A randomized phase II trial of the Trans-Tasman Radiation Oncology Group (TROG 98.02). *J. Clin. Oncol.* **2005**, *23*, 79–87.

(19) Le, Q.-T.; Taira, A.; Budenz, S.; Dorie, M. J.; Goffinet, D. R.; Fee, W. E.; Goode, R.; Bloch, D.; Koong, A.; Brown, J. M.; Pinto, H. A. Mature results from a randomized phase II trial of cisplatin plus 5-fluouracil and radiotherapy with or without tirapazamine in patients with respectable stage IV head and neck squamous cell carcinomas. *Cancer* **2006**, *106*, 1940–1949.

(20) Rischin, D.; Hicks, R. J.; Fisher, R.; Binns, D.; Corry, J.; Porceddu, S.; Peters, L. J. Prognostic significance of [^{18}F]-misonidazole positron emission tomography-detected tumor hypoxia in patients with advanced head and neck cancer randomly assigned to chemoradiation with or without tirapazamine: a substudy of Trans-Tasman Radiation Oncology Group study 98.02. *J. Clin. Oncol.* **2006**, *24*, 2098–2104.

(21) Patterson, A. V.; Saunders, M. P.; Chinje, E. C.; Patterson, L. H.; Stratford, I. J. Enzymology of tirapazamine metabolism: A review. *Anti-Cancer Drug Des.* **1998**, *13*, 541–573.

(22) Baker, M. A.; Zeman, E. M.; Hirst, V. K.; Brown, J. M. Metabolism of SR 4233 by Chinese hamster ovary cells: Basis of selective hypoxic cytotoxicity. *Cancer Res.* **1988**, *48*, 5947–5952.

(23) Priyadarsini, K. I.; Tracy, M.; Wardman, P. The one electron reduction potential of 3-amino-1,2,4-benzotriazine 1,4-dioxide (Tirapazamine): A hypoxia-selective bioreductive drug. *Free Radical Res.* **1996**, *25*, 393–399.

(24) Daniels, J. S.; Gates, K. S. DNA cleavage by the antitumor agent 3-amino-1,2,4-benzotriazine 1,4-dioxide (SR4233). Evidence for involvement of hydroxyl radical. *J. Am. Chem. Soc.* **1996**, *118*, 3380–3385.

(25) Anderson, R. F.; Shinde, S. S.; Hay, M. P.; Gamage, S. A.; Denny, W. A. Activation of 3-amino-1,2,4-benzotriazine 1,4-dioxide antitumor agents to oxidizing species following their one-electron reduction. *J. Am. Chem. Soc.* **2003**, *125*, 748–756.

(26) Shinde, S. S.; Anderson, R. F.; Hay, M. P.; Gamage, S. A.; Denny, W. A. Oxidation of 2-deoxyribose by benzotriazinyl radicals of antitumor 3-amino-1,2,4-benzotriazine 1,4-dioxides. *J. Am. Chem. Soc.* **2004**, *126*, 7853–7864.

(27) Jones, G. D. D.; Weinfeld, M. Dual action of tirapazamine in the induction of DNA strand breaks. *Cancer Res.* **1996**, *56*, 1584–1590.

(28) Siim, B. G.; van Zijl, P. L.; Brown, J. M. Tirapazamine-induced DNA damage measured using the comet assay correlates with cytotoxicity towards hypoxic tumour cells in vitro. *Br. J. Cancer* **1996**, *73*, 952–960.

(29) Siim, B. G.; Menke, D. R.; Dorie, M. J.; Brown, J. M. Tirapazamine-induced cytotoxicity and DNA damage in transplanted tumors: Relationship to tumor hypoxia. *Cancer Res.* **1997**, *57*, 2922–2928.

(30) Daniels, J. S.; Gates, K. S.; Tronche, C.; Greenberg, M. M. Direct evidence for bimodal DNA damage induced by tirapazamine. *Chem. Res. Toxicol.* **1998**, *11*, 1254–1257.

(31) Hwang, J.-T.; Greenberg, M. M.; Fuchs, T.; Gates, K. S. Reaction of the hypoxia-selective antitumor agent tirapazamine with a C1′-radical in single-stranded and double-stranded DNA: The drug and its metabolites can serve as surrogates for molecular oxygen in radical-mediated DNA damage reactions. *Biochemistry* **1999**, *38*, 14248–14255.

(32) Wang, J.; Biedermann, K. A.; Brown, J. M. Repair of DNA and chromosome breaks in cells exposed to SR 4233 under hypoxia or to ionizing radiation. *Cancer Res.* **1992**, *52*, 4473–4477.

(33) Siim, B. G.; Pruijn, F. B.; Sturman, J. R.; Hogg, A.; Hay, M. P.; Brown, J. M.; Wilson, W. R. Selective potentiation of the hypoxic cytotoxicity of tirapazamine by its 1-*N*-oxide metabolite SR 4317. *Cancer Res.* **2004**, *64*, 736–742.

(34) Peters, K. B.; Brown, J. M. Tirapazamine: A hypoxia-activated topoisomerase II poison. *Cancer Res.* **2002**, *62*, 5248–5283.

(35) Doherty, N.; Hancock, S. L.; Kaye, S.; Coleman, C. N.; Shulman, L.; Marquez, C.; Mariscal, C.; Rampling, R.; Senan, S.; Roemeling, R. V. Muscle cramping in phase I clinical trials of tirapazamine (SR 4233) with and without radiation. *Int. J. Radiat. Oncol., Biol., Phys.* **1994**, *29*, 379–382.

(36) Durand, R. E.; Olive, P. L. Physiologic and cytotoxic effects of tirapazamine in tumor-bearing mice. *Radiat. Oncol. Invest.* **1997**, *5*, 213–219.

(37) Durand, R. E.; Olive, P. L. Evaluation of bioreductive drugs in multicell spheroids. *Int. J. Radiat. Oncol., Biol., Phys.* **1992**, *22*, 689–692.

(38) Hicks, K. O.; Fleming, Y.; Siim, B. G.; Koch, C. J.; Wilson, W. R. Extravascular diffusion of tirapazamine: Effect of metabolic consumption assessed using the multicellular layer model. *Int. J. Radiat. Oncol., Biol., Phys.* **1998**, *42*, 641–649.

(39) Kyle, A. H.; Minchinton, A. I. Measurement of delivery and metabolism of tirapazamine to tumour tissue using the multilayered cell culture model. *Cancer Chemother. Pharmacol.* **1999**, *43*, 213–220.

(40) Baguley, B. C.; Hicks, K. O.; Wilson, W. R. Tumour cell cultures in drug development. In *Anticancer Drug Development*; Baguley, B. C., Kerr, D. J., Eds.; Academic Press: San Diego, CA, 2002; pp 269–284.

(41) Hicks, K. O.; Pruijn, F. B.; Sturman, J. R.; Denny, W. A.; Wilson, W. R. Multicellular resistance to tirapazamine is due to restricted extravascular transport: A pharmacokinetic/pharmacodynamic study in multicellular layers. *Cancer Res.* **2003**, *63*, 5970–5977.

(42) Hicks, K. O.; Siim, B. G.; Pruijn, F. B.; Wilson, W. R. Oxygen dependence of the metabolic activation and cytotoxicity of tirapazamine: Implications for extravascular transport and activity in tumors. *Radiat. Res.* **2004**, *161*, 656–666.

(43) Hicks, K. O.; Pruijn, F. B.; Secomb, T. W.; Hay, M. P.; Hsu, R.; Brown, J. M.; Denny, W. A.; Dewhirst, M. W.; Wilson, W. R. Use of three-dimensional tissue cultures to model extravascular transport and predict in vivo activity of hypoxia-targeted anticancer drugs. *J. Natl. Cancer Inst.* **2006**, *98*, 1118–1128.

(44) Hicks, K. O.; Fleming, Y.; Siim, B. G.; Koch, C. J.; Wilson, W. R. Extravascular diffusion of tirapazamine: Effect of metabolic consumption assessed using the multicellular layer model. *Int. J. Radiat. Oncol., Biol., Phys.* **1998**, *42*, 641–649.
(45) Pruijn, F. B.; Sturman, J.; Liyanage, S.; Hicks, K. O.; Hay, M. P.; Wilson, W. R. Extravascular transport of drugs in tumor tissue: Effect of lipophilicity on diffusion of tirapazamine analogues in multicellular layer cultures. *J. Med. Chem.* **2005**, *48*, 1079–1087.
(46) Hicks, K. O.; Myint, H.; Patterson, A. V.; Pruijn, F. B.; Siim, B. G.; Patel, K.; Wilson, W. R. Oxygen dependence and extravascular transport of hypoxia-activated prodrugs: comparison of the dinitrobenzamide mustard PR-104A and tirapazamine. *Int. J. Radiat. Oncol., Biol., Phys.* 2007, *69,* 560–571.
(47) Kelson, A. B.; McNamara, J. P.; Pandey, A.; Ryan, K. J.; Dorie, M. J.; McAfee, P. A.; Menke, D. R.; Brown, J. M.; Tracy, M. 1,2,4-Benzotriazine 1,4-dioxides. An important class of hypoxic cytotoxins with antitumor activity. *Anti-Cancer Drug Des.* **1998**, *13*, 575–592.
(48) Hay, M. P.; Gamage, S. A.; Kovacs, M. S.; Pruijn, F. B.; Anderson, R. F.; Patterson, A. V.; Wilson, W. R.; Brown, J. M.; Denny, W. A. Structure−activity relationships of 1,2,4-benzotriazine 1,4-dioxides as hypoxia-selective analogues of tirapazamine. *J. Med. Chem.* **2003**, *46*, 169–182.
(49) Arndt, F. Ring-closing between nitro and amino groups forming triazines. *Ber.* **1913**, *46*, 3522–3529.
(50) Siim, B. G.; Hicks, K. O.; Pullen, S. M.; van Zijl, P. L.; Denny, W. A.; Wilson, W. R. Comparison of aromatic and tertiary amine *N*-oxides of acridine DNA intercalators as bioreductive drugs—Cytotoxicity, DNA binding, cellular uptake, and metabolism. *Biochem. Pharmacol.* **2000**, *60*, 969–978.
(51) Pruijn, F. B.; Patel, K.; Liyanage, H. D. S.; Hicks, K. O.; Hay, M. P.; Wilson, W. R. Unpublished results.
(52) Dedrick, R. L.; Flessner, M. F. Pharmacokinetic problems in peritoneal drug administration: Tissue penetration and surface exposure. *J. Natl. Cancer Inst.* **1997**, *89*, 480–487.
(53) The computational algorithm is available at http://jnci.oxfordjournals.org/cgi/content/full/98/16/1118/DC1.
(54) Cliffe, S.; Taylor, M. L.; Rutland, M.; Baguley, B. C.; Hill, R. P.; Wilson, W. R. Combining bioreductive drugs (SR 4233 or SN 23862) with the vasoactive agents flavone acetic acid or 5,6-dimethylxanthenone acetic acid. *Int. J. Radiat. Oncol., Biol., Phys.* **1994**, *29*, 373–377.
(55) Mason, J. C.; Tennant, G. Heterocyclic *N*-oxides. Part VI. Synthesis and nuclear magnetic resonance spectra of 3-aminobenzo-1,2,4-triazines and their mono- and di-*N*-oxides. *J. Chem. Soc. B* **1970**, 911–916.
(56) Hicks, K. O.; Pruijn, F. B.; Baguley, B. C.; Wilson, W. R. Extravascular transport of the DNA intercalator and topoisomerase poison *N*-[2-(dimethylamino)ethyl]acridine-4-carboxamide (DACA): Diffusion and metabolism in multicellular layers of tumor cells. *J. Pharmacol. Exp. Ther.* **2001**, *297*, 1088–1098.
(57) Siim, B. G.; Atwell, G. J.; Wilson, W. R. Oxygen dependence of the cytotoxicity and metabolic activation of 4-alkylamino-5-nitroquinoline bioreductive drugs. *Br. J. Cancer* **1994**, *70*, 596–603.
(58) Skehan, P.; Storeng, R.; Scudiero, D.; Monks, A.; McMahon, J.; Vistica, D.; Warren, J. T.; Bokesch, H.; Kenney, S.; Boyd, M. R. New colorimetric cytotoxicity assay for anticancer-drug screening. *J. Natl. Cancer Inst.* **1990**, *82*, 1107–1112.
(59) Wilson, W. R.; Pullen, S. M.; Hogg, A.; Hobbs, S. M.; Pruijn, F. B.; Hicks, K. O. In vitro and in vivo models for evaluation of GDEPT: Quantifying bystander killing in cell cultures and tumors. In *Suicide Gene Therapy: Methods and Protocols for Cancer*; Springer, C. J., Ed.; Humana Press: Totowa, NJ, 2003; pp 403–432.

JM070670G